JACS
JOURNAL OF THE AMERICAN CHEMICAL SOCIETY
pubs.acs.org/JACS
Communication

Covalent C−N Bond Formation through a Surface Catalyzed Thermal Cyclodehydrogenation

Ilya Piskun,[○] Raymond Blackwell,[○] Joaquim Jornet-Somoza, Fangzhou Zhao, Angel Rubio, Steven G. Louie, and Felix R. Fischer*

Cite This: J. Am. Chem. Soc. 2020, 142, 3696−3700
Read Online
ACCESS | Metrics & More | Article Recommendations | Supporting Information

ABSTRACT: The integration of substitutional dopants at predetermined positions along the hexagonal lattice of graphene-derived polycyclic aromatic hydrocarbons is a critical tool in the design of functional electronic materials. Here, we report the unusually mild thermally induced oxidative cyclodehydrogenation of dianthryl pyrazino[2,3-*g*]quinoxalines to form the four covalent C−N bonds in tetraazateranthene on Au(111) and Ag(111) surfaces. Bond-resolved scanning probe microscopy, differential conductance spectroscopy, along with first-principles calculations unambiguously confirm the structural assignment. Detailed mechanistic analysis based on ab initio density functional theory calculations reveals a stepwise mechanism featuring a rate determining barrier of only $\Delta E^{\ddagger}$ = 0.6 eV, consistent with the experimentally observed reaction conditions.

Oxidative cyclodehydrogenation reactions have found extensive use in the synthesis of extended polycyclic aromatic hydrocarbons (PAH). Solution-based Scholl and Kovacic reactions among many others, which rely on Lewis acid/oxidant combinations, have widely been used to induce the intramolecular cyclodehydrogenation of carefully designed *oligo*-arene precursors into extended PAHs.[1] The emergence of bond-resolved SPM characterization techniques along with an expanded understanding of surface catalyzed reaction mechanisms[2] has even provided access to PAH structures featuring high-energy ground states,[3−5] open-shell electron configurations,[6] and highly reactive unsaturated spin systems.[7] One of the most common approaches relies on a thermally induced 6π electrocyclization of an *oligo*-arene precursor that is either preceded or followed by the transfer of two hydrogen atoms to the underlying metal surface.[8] The thermal activation barrier for this process varies with the underlying substrate and to a lesser extent with the structure of the molecular precursor, but generally requires annealing temperatures ranging between 200 and 450 °C.[9,10] While this approach has been broadly applied to the formation of covalent C−C bonds on Au, Ag, and Cu surfaces, the analogous reaction establishing covalent C−heteroatom bonds has never been observed. While a wide variety of heteroatoms (e.g., N, S, O, B) have been used to replace C−H groups along the edges of PAHs,[11−14] the electronically much more interesting substitution of trigonal planar carbon atoms at the center of extended π-system remains rare. Access to these backbone-substituted PAHs has exclusively relied on the pre-assembly of all carbon−heteroatom bonds present in the product at the *oligo*-arene precursor stage.[15−19]

We herein report the first example of a surface catalyzed cyclodehydrogenation that leads to the formation of covalent C−N bonds in an extended PAH. The thermally induced intramolecular cyclodehydrogenation of pyrazino[2,3-*g*]-quinoxalines **2a−c** (Scheme 1) on Au(111) or Ag(111) surfaces proceeds at unusually low temperatures and leads to the formation of four covalent C−N bonds in the tetraazateranthene **1**. The synthesis of dianthryl pyrazino[2,3-*g*]quinoxalines **2a−c** is depicted in Scheme 2. Condensation of 2,5-dihydroxy-1,4-benzoquinone (**3**) with ethylenediamine followed by catalytic dehydrogenation gives pyrazino[2,3-*g*]quinoxaline (**4**) in two steps. Dibromination of **4** with NBS and subsequent Suzuki−Miyaura cross-coupling with 2-(anthracen-9-yl)-4,4,5,5-tetramethyl-1,3,2-dioxaborolane yields the parent dianthryl pyrazino[2,3-*g*]quinoxaline **2a**. While pyrazino[2,3-*g*]quinoxaline **2b** can be obtained through direct bromination with *N*-bromosuccinimide in 70% yield, a two-step sequence of Miyaura borylation followed by treatment of the intermediate mixture of pinacol boronic esters with copper iodide is required to obtain the diiodinated pyrazino[2,3-*g*]quinoxaline **2c** albeit in a lower yield (∼ 7% over two steps).

Pyrazino[2,3-*g*]quinoxalines **2a−c** were deposited from a Knudsen cell evaporator in ultrahigh vacuum onto Au(111)

Scheme 1. Surface Supported Thermal Cyclodehydrogenation of 2a−c on Au(111) or Ag(111) to Give Tetraazateranthene 1

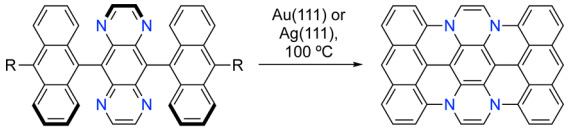

2a R = H
2b R = Br
2c R = I

1

Received: December 15, 2019
Published: February 11, 2020

https://dx.doi.org/10.1021/jacs.9b13507
J. Am. Chem. Soc. 2020, 142, 3696−3700

Scheme 2. Synthesis of Pyrazino[2,3-*g*]quinoxalines 2a−c

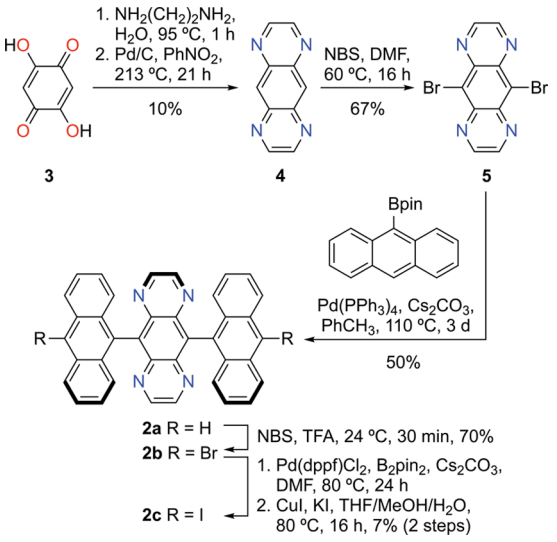

and Ag(111) surfaces held at 24 °C. Figure 1A shows a representative STM topographic image (5 K) of self-assembled multilayer islands of **2a** on a Au(111) crystal surface. Isolated molecules of **2a** adsorb preferentially in a conformation that places the anthracenyl groups at either end of the molecule nearly coplanar to the underlying surface (Figure S1). One side of the central pyrazino[2,3-*g*]quinoxaline ring protrudes high above the plane of the molecule and appears as a characteristic bright feature in the topographic image in Figure 1B. Annealing of molecule decorated surfaces at temperatures as low as 75−100 °C for 15 min induces a thermal cyclodehydrogenation of all *peri*-positions to form tetraazateranthene **1** (Figure 1C,D). STM images on Au(111) or Ag(111) reveal a submonolayer coverage of the surface with discrete rectangular structures measuring 0.95 ± 0.05 nm, 1.20 ± 0.15 nm, and 0.19 ± 0.02 nm in width, length, and height, respectively (Figure 1E). There is no observable difference in cyclodehydrogenation conditions between Au(111) and Ag(111). Bond-resolved STM (BRSTM) imaging, wherein the STM tip is functionalized with a carbon monoxide molecule to conduct imaging in the Pauli repulsive regime,[20,21] confirms the tentative structural assignment and shows the fully fused core along with the four covalent C−N bonds of tetraazateranthene **1** (Figure 1F). Large-area scans on Au(111) and Ag(111) highlight the remarkable selectivity and the high yield of this transformation (Figure 1C,D). Even in the presence of the thermally labile C−Br or C−I bonds in **2b** and **2c**, the cyclodehydrogenation to form **1** proceeds at temperatures <100 °C. The coplanar conformation adopted by the anthracene and the pyrazino[2,3-*g*]quinoxaline rings in the fully cyclodehydrogenated core of **1** precludes the expected radical step-growth polymerization along the zigzag edges on the surface (Figure S2) and instead only yields the exhaustive dehalogenation product tetraazateranthene **1**.

Differential conductance (dI/dV) point spectra collected above the nitrogen atoms along the armchair edge of tetraazateranthene **1** (inset Figure 2) reveals two characteristic features associated with an occupied and an unoccupied state at a sample bias of −0.6 V and +1.6 V, respectively (Figure 2). The dI/dV maps recorded at the corresponding energies show the spatial distribution of the local density of states (LDOS) across the surface of the adsorbed molecule. In an effort to

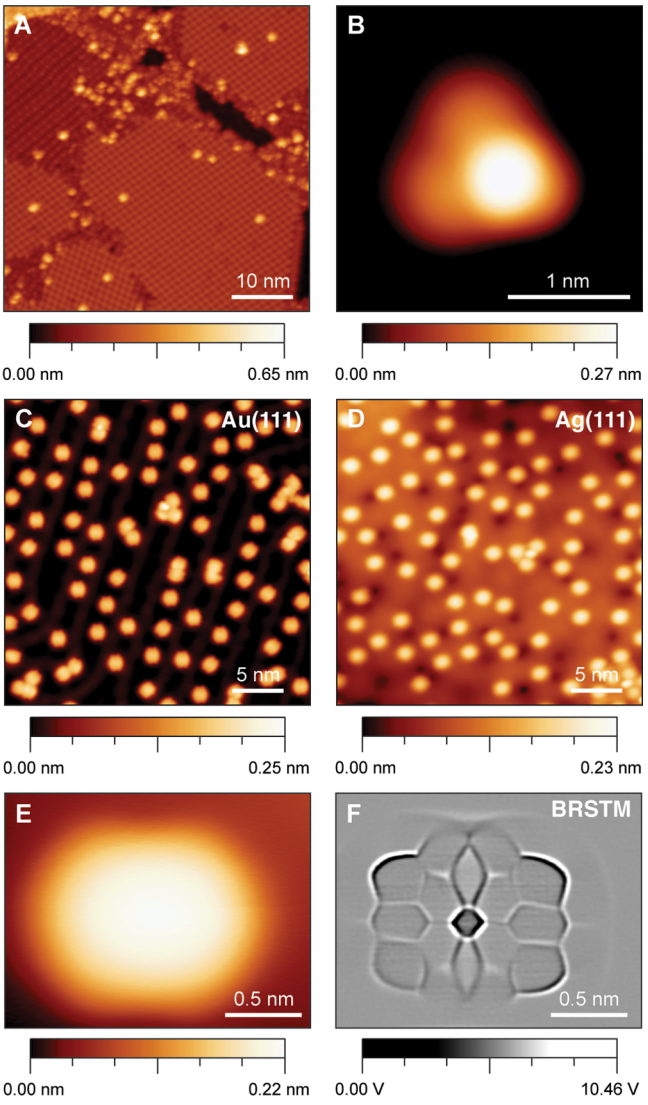

Figure 1. STM topographic image of (A) self-assembled islands and (B) an isolated molecule of **2a** on a Au(111) surface. STM topographic image of (C) a Au(111) and (D) a Ag(111) surface after annealing to 100 °C showing the clean transformation of **2a** to **1** (dark depressions in (D) are due to missing atoms in the lattice of the Ag(111) surface following the sputtering and annealing cycles). (E) STM topographic and (F) Laplace filtered BRSTM image of fully cyclized tetraazateranthene **1** on Au(111). ((A)−(E): V_s = 50 mV I_t = 20 pA; (F) V_s = 0 mV, f_V: 455 Hz, ΔV_s = 10 mV)

assign the peaks in the differential conductance spectra to molecular frontier orbitals, we performed density functional theory (DFT) calculations with local density approximation (LDA)[22] as well as a GW calculation which incorporates the electron self-energy in a many-electron Green function approach.[23,24] The peak at −0.6 V closely resembles the projection of the HOMO−2 orbital of tetraazateranthene, while the broader feature at +1.6 V is best represented by a superposition of the LUMO and the LUMO+1 orbitals. While the degeneracy between LUMO and LUMO+1 is not immediately apparent from calculations within the LDA framework alone, quasiparticle calculations using the GW correction confirm that LUMO and LUMO+1 of **1** are separated by ΔE < 50 meV. An analysis of wave function symmetry of the frontier orbitals of tetraazaanthene **1**

https://dx.doi.org/10.1021/jacs.9b13507
J. Am. Chem. Soc. 2020, 142, 3696−3700

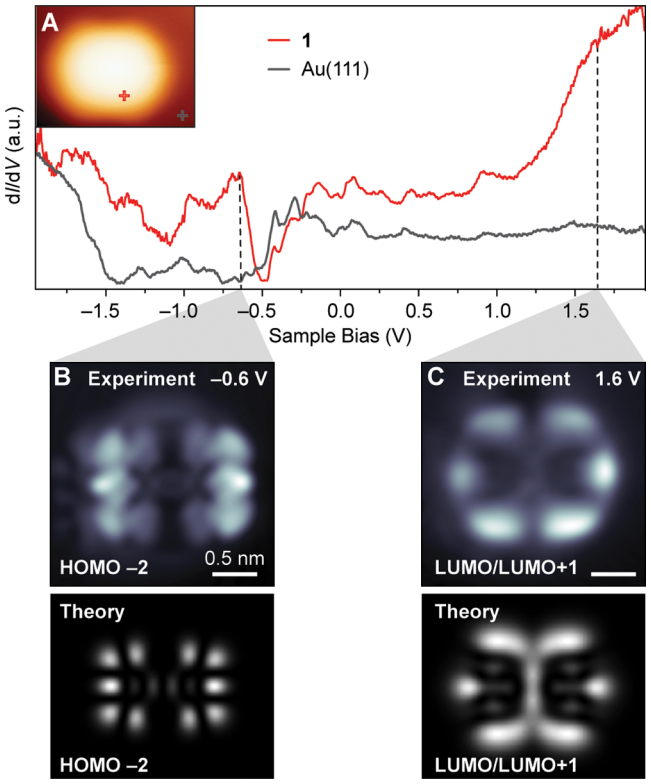

Figure 2. (A) STM dI/dV point spectrum of **1** on Au(111). Experimental dI/dV spatial maps and calculated position dependence of the LDOS map of states with energy fixed at (B) V_s = −0.6 V (I_t = 0.60 nA) and (C) V_s = +1.6 V (I_t = 0.75 nA). Calculated lateral spatial distribution of LDOS at fixed energy is evaluated at a height of 4 Å above the plane.

calculated in the gas phase (Figure S3) suggests strong hybridization of HOMO and HOMO−1 states with the underlying Au(111) or Ag(111) substrate. The resulting significant broadening prevents an unambiguous assignment of the HOMO and HOMO−1 feature in the dI/dV spectrum.

Further insight into the mechanism of the surface-assisted cyclodehydrogenation of **2a** including the formation of four C−N bonds was obtained from *ab initio* calculations using the all-electron FHI-aims code.[25] We determined the reaction-energy landscape including all transient intermediates and transition states using DFT at the PBE+vdW+ZORA level for four discrete cyclization sequences (Figures S4−S8). While the calculated rate determining transition states range between $\Delta E^{\ddagger}$ = 0.6 and 3.5 eV above the starting materials (**2a** physisorbed on Au(111)), in the following discussion, we will focus only on the most plausible mechanism involving the lowest overall activation barrier (Figure 3a).

An initial step involving the concerted or stepwise (Figure S8) formation of two C−N bonds between the physisorbed side of the pyrazino[2,3-*g*]quinoxaline and the two anthracene units represents the rate-determining transition state and is associated with an activation barrier of $\Delta E^{\ddagger}$ = +0.6 eV. The transition state structure **TS1** is characterized by an allylic diradical that undergoes a rapid suprafacial [1,2] hydrogen shift (red H atoms in **TS1**) to give the stabilized benzylic radical intermediate **Int1**. The subsequent transfer of the two hydrogen atoms closest to the substrate (black H atoms in **Int1**) to the Au(111) surface is virtually barrierless ($\Delta E^{\ddagger}$ = +0.3 eV) and leads to the partially cyclodehydrogentated

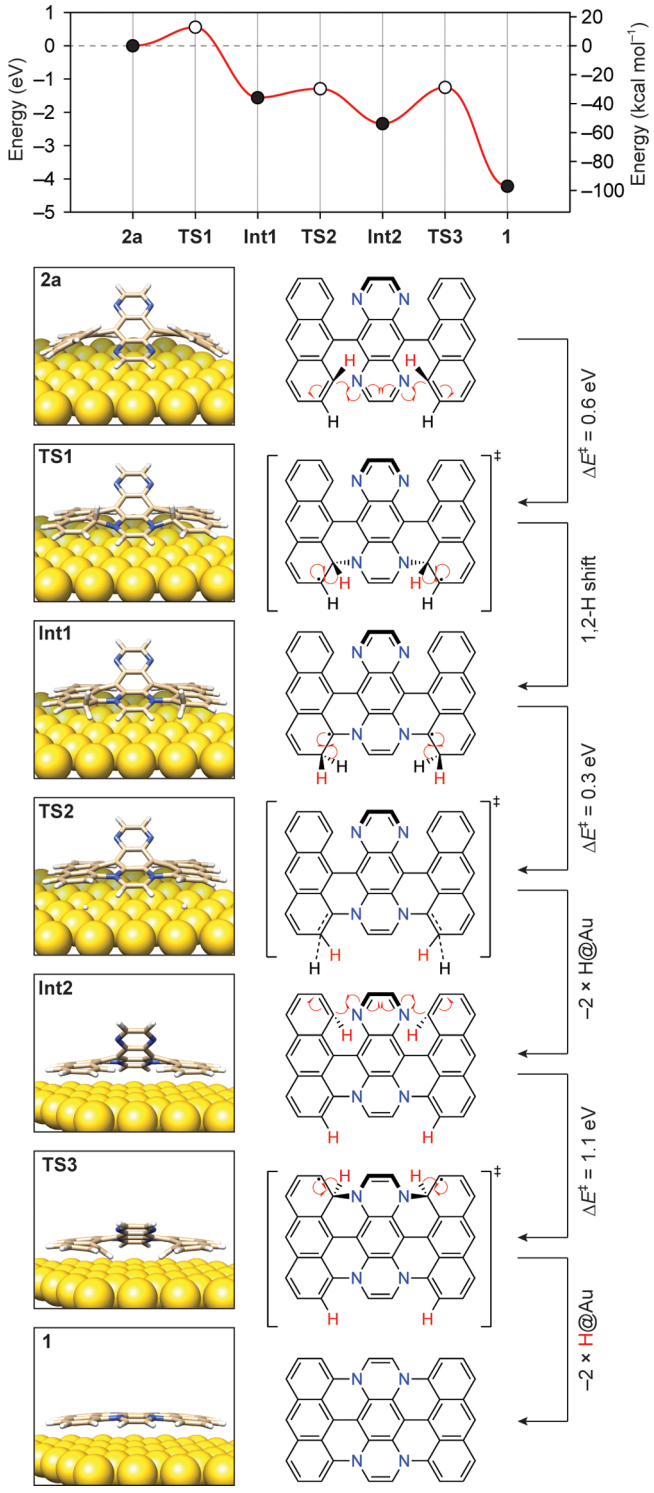

Figure 3. Calculated energy diagram for the stepwise cyclodehydrogenation of **2a** to **1**. The graph shows the ab initio energy landscape for intermediates and transition states along the reaction pathway from **2a** to **1**. Calculated activation energies are shown next to the reaction arrows.

intermediate **Int2** featuring two out of the four C−N bonds in the tetraazateranthene **1**. It is important to point out that we have never observed the partially cyclized intermediate **Int2** on the surface of Au(111) or Ag(111). The only two unimolecular species that could be imaged throughout the reaction are the as-deposited starting material **2a** (or **2b**,**c**) and the fully

https://dx.doi.org/10.1021/jacs.9b13507
J. Am. Chem. Soc. 2020, 142, 3696−3700

cyclized product **1** following the annealing step (Figure S2). The cyclization of the remaining pyrazino[2,3-*g*]quinoxaline wing protruding from the surface proceeds through a single transition state, albeit with a higher activation barrier ($\Delta E^{\ddagger}$ = +1.1 eV). The two remaining C−N bonds are formed through an approach of the pyrazino[2,3-*g*]quinoxaline wing from above the plane of the anthracenes, placing the red hydrogen atoms in the allyl diradical-like transition state **TS3** in a position pointing directly toward the underlying Au(111) surface. Direct transfer of these hydrogen atoms to the surface yields the fully cyclized tetrateranthene **1**.

In summary, we report the experimental demonstration and detailed mechanistic investigation of an intramolecular cyclodehydrogenation that leads to the formation of four covalent C−N bonds on Au(111) and Ag(111) surfaces. SPM imaging reveals that molecular precursors **2a−c** adsorb in a chairlike conformation on metal substrates and undergo a clean conversion to tetraazateranthene **1** under mild conditions. BRSTM and differential conductance spectroscopy unambiguously confirm the structural assignment. Mechanistic analysis based on ab initio DFT calculations reveals the most likely stepwise mechanism featuring a rate-determining barrier of only $\Delta E^{\ddagger}$ = 0.6 eV, consistent with the experimentally observed reaction conditions (T = 75−100 °C). This work expands our mechanistic understanding of oxidative C−N bond formation reactions on metal surfaces and provides a useful tool for the incorporation of substitutional heteroatom dopants into the extended π-backbone of bottom-up synthesized nanographene.

■ ASSOCIATED CONTENT

Supporting Information

The Supporting Information is available free of charge at https://pubs.acs.org/doi/10.1021/jacs.9b13507.

Figures S1−S8, methods and instrumentation, synthetic procedures for **2a−c**, computational details, and NMR spectra (Figures S9 to S15) (PDF)

■ AUTHOR INFORMATION

Corresponding Author

Felix R. Fischer − *Department of Chemistry, University of California, Berkeley, California 94720, United States; Materials Sciences Division, Lawrence Berkeley National Laboratory, Berkeley, California 94720, United States; Kavli Energy NanoSciences Institute at the University of California Berkeley and the Lawrence Berkeley National Laboratory, Berkeley, California 94720, United States;* orcid.org/0000-0003-4723-3111; Email: ffischer@berkeley.edu

Authors

Ilya Piskun − *Department of Chemistry, University of California, Berkeley, California 94720, United States*

Raymond Blackwell − *Department of Chemistry, University of California, Berkeley, California 94720, United States;* orcid.org/0000-0002-3501-9444

Joaquim Jornet-Somoza − *Nano-Bio Spectroscopy Group and ETSF, Universidad del País Vasco UPV/EHU, E-20018 Donostia, Spain; Max Planck Institute for the Structure and Dynamics of Matter, 22761 Hamburg, Germany;* orcid.org/0000-0002-6721-1393

Fangzhou Zhao − *Department of Physics, University of California, Berkeley, California 94720, United States; Materials Sciences Division, Lawrence Berkeley National Laboratory, Berkeley, California 94720, United States;* orcid.org/0000-0001-7355-7406

Angel Rubio − *Nano-Bio Spectroscopy Group and ETSF, Universidad del País Vasco UPV/EHU, E-20018 Donostia, Spain; Max Planck Institute for the Structure and Dynamics of Matter, 22761 Hamburg, Germany; Center for Computational Quantum Physics (CCQ), The Flatiron Institute, New York, New York 10010, United States;* orcid.org/0000-0003-2060-3151

Steven G. Louie − *Department of Physics, University of California, Berkeley, California 94720, United States; Materials Sciences Division, Lawrence Berkeley National Laboratory, Berkeley, California 94720, United States;* orcid.org/0000-0003-0622-0170

Complete contact information is available at: https://pubs.acs.org/10.1021/jacs.9b13507

Author Contributions

○These authors contributed equally.

Notes

The authors declare no competing financial interest.

■ ACKNOWLEDGMENTS

Research was supported by the Office of Naval Research MURI Program N00014-16-1-2921 (design and synthesis of molecular precursors and theoretical analyses), the Center for Energy Efficient Electronics NSF award 0939514 (SPM and STS), and the National Science Foundation under grant DMR-1926004 (DFT and GW calculations). R.B. acknowledges support through a National Science Foundation Graduate Research Fellowship under grant DGE-1106400. A.R. was supported by the European Research Council (ERC-2015-AdG694097) and Grupos Consolidados (IT1249-19). Berkeley NMR Facility is supported in part by NIH grants 1S10RR016634-01, SRR023679A, and S10OD024998. J.J.S. acknowledges funding from the European Union Horizon 2020 research and innovation program under the Marie Sklodowska-Curie grant agreement no. 795246-StrongLights.

■ REFERENCES

(1) Grzybowski, M.; Skonieczny, K.; Butenschon, H.; Gryko, D. T. Comparison of Oxidative Aromatic Coupling and the Scholl Reaction. *Angew. Chem., Int. Ed.* **2013**, *52*, 9900−9930.

(2) de Oteyza, D. G.; Gorman, P.; Chen, Y.-C.; Wickenburg, S.; Riss, A.; Mowbray, D. J.; Etkin, G.; Pedramrazi, Z.; Tsai, H.-Z.; Rubio, A.; Crommie, M. F.; Fischer, F. R. Direct Imaging of Covalent Bond Structure in Single-Molecule Chemical Reactions. *Science* **2013**, *340*, 1434−1437.

(3) Rogers, C.; Chen, C.; Pedramrazi, Z.; Omrani, A. A.; Tsai, H.; Jung, H. S.; Lin, S.; Crommie, M. F.; Fischer, F. R. Closing the Nanographene Gap: Surface-Assisted Synthesis of Peripentacene from 6,6′-Bipentacene Precursors. *Angew. Chem., Int. Ed.* **2015**, *54*, 15143−15146.

(4) Pozo, I.; Majzik, Z.; Pavliček, N.; Melle-Franco, M.; Guitián, E.; Peña, D.; Gross, L.; Pérez, D. Revisiting Kekulene: Synthesis and Single-Molecule Imaging. *J. Am. Chem. Soc.* **2019**, *141*, 15488−15493.

(5) Zuzak, R.; Dorel, R.; Kolmer, M.; Szymonski, M.; Godlewski, S.; Echavarren, A. M. Higher Acenes by On-Surface Dehydrogenation: From Heptacene to Undecacene. *Angew. Chem., Int. Ed.* **2018**, *57*, 10500−10505.

(6) Majzik, Z.; Pavlicek, N.; Vilas-Varela, M.; Perez, D.; Moll, N.; Guitian, E.; Meyer, G.; Pena, D.; Gross, L. Studying an Antiaromatic

Polycyclic Hydrocarbon Adsorbed on Different Surfaces. *Nat. Commun.* **2018**, *9*, 1198.
(7) Pavliček, N.; Mistry, A.; Majzik, Z.; Moll, N.; Meyer, G.; Fox, D. J.; Gross, L. Synthesis and Characterization of Triangulene. *Nat. Nanotechnol.* **2017**, *12*, 308−311.
(8) Treier, M.; Pignedoli, C. A.; Laino, T.; Rieger, R.; Müllen, K.; Passerone, D.; Fasel, R. Surface-Assisted Cyclodehydrogenation Provides a Synthetic Route Towards Easily Processable and Chemically Tailored Nanographenes. *Nat. Chem.* **2011**, *3*, 61−67.
(9) Bjork, J.; Stafstrom, S.; Hanke, F. Zipping Up: Cooperativity Drives the Synthesis of Graphene Nanoribbons. *J. Am. Chem. Soc.* **2011**, *133*, 14884−14887.
(10) De Oteyza, D. G.; Clair, S. Controlling a Chemical Reaction on a Surface: Tools and Strategies for On-surface Synthesis. *Chem. Rev.* **2019**, *119*, 4717−4776.
(11) Bronner, C.; Stremlau, S.; Gille, M.; Brausse, F.; Haase, A.; Hecht, S.; Tegeder, P. Aligning the Band Gap of Graphene Nanoribbons by Monomer Doping. *Angew. Chem., Int. Ed.* **2013**, *52*, 4422−4425.
(12) Wang, X.-Y.; Urgel, J. I.; Barin, G. B.; Eimre, K.; Di Giovannantonio, M.; Milani, A.; Tommasini, M.; Pignedoli, C. A.; Ruffieux, P.; Feng, X.; Fasel, R.; Müllen, K.; Narita, A. Bottom-Up Synthesis of Heteroatom-Doped Chiral Graphene Nanoribbons. *J. Am. Chem. Soc.* **2018**, *140*, 9104−9107.
(13) Durr, R. A.; Haberer, D.; Lee, Y.-L.; Blackwell, R.; Kalayjian, A. M.; Marangoni, T.; Ihm, J.; Louie, S. G.; Fischer, F. R. Orbitally Matched Edge-Doping in Graphene Nanoribbons. *J. Am. Chem. Soc.* **2018**, *140*, 807−813.
(14) Wang, X.-Y.; Yao, X.; Narita, A.; Müllen, K. Heteroatom-Doped Nanographenes with Structural Precision. *Acc. Chem. Res.* **2019**, *52*, 2491−2505.
(15) Wang, X.-Y.; Richter, M.; He, Y.; Björk, J.; Riss, A.; Rajesh, R.; Garnica, M.; Hennersdorf, F.; Weigand, J. J.; Narita, A.; Berger, R.; Feng, X.; Auwärter, W.; Barth, J. V.; Palma, C.-A.; Müllen, K. Exploration of Pyrazine-Embedded Antiaromatic Polycyclic Hydrocarbons Generated by Solution and On-Surface Azomethine Ylide Homocoupling. *Nat. Commun.* **2017**, *8*, 1948.
(16) Kawai, S.; Nakatsuka, S.; Hatakeyama, T.; Pawlak, R.; Meier, T.; Tracey, J.; Meyer, E.; Foster, A. S. Multiple heteroatom substitution to graphene nanoribbon. *Sci. Adv.* **2018**, *4*, eaar7181.
(17) Ciccullo, F.; Calzolari, A.; Pis, I.; Savu, S.-A.; Krieg, M.; Bettinger, H. F.; Magnano, E.; Chasse, T.; Casu, M. B. A Quasi-Free-Standing Single Layer of a B_3N_3-doped Nanographene Molecule Deposited on Au(111) Single Crystals. *J. Phys. Chem. C* **2016**, *120*, 17645−17651.
(18) Cloke, R. R.; Marangoni, T.; Nguyen, G. D.; Joshi, T.; Rizzo, D. J.; Bronner, C.; Cao, T.; Louie, S. G.; Crommie, M. F.; Fischer, F. R. Site-Specific Substitutional Boron Doping of Semiconducting Armchair Graphene Nanoribbons. *J. Am. Chem. Soc.* **2015**, *137*, 8872−8875.
(19) Kawai, S.; Saito, S.; Osumi, S.; Yamaguchi, S.; Foster, A. S.; Spijker, P.; Meyer, E. Atomically Controlled Substitutional Boron Doping of Graphene Nanoribbons. *Nat. Commun.* **2015**, *6*, 8098.
(20) Weiss, C.; Wagner, C.; Kleimann, C.; Rohlfing, M.; Tautz, F. S.; Temirov, R. Imaging Pauli Repulsion in Scanning Tunneling Microscopy. *Phys. Rev. Lett.* **2010**, *105*, 086103.
(21) Hapala, P.; Kichin, G.; Wagner, C.; Tautz, F. S.; Temirov, R.; Jelinek, P. Mechanism of High Resolution STM/AFM Imaging with Functionalized Tips. *Phys. Rev. B: Condens. Matter Mater. Phys.* **2014**, *90*, 085421.
(22) Giannozzi, P.; Baroni, S.; Bonini, N.; Calandra, M.; Car, R.; Cavazzoni, C.; Ceresoli, D.; Chiarotti, G. L; Cococcioni, M.; Dabo, I.; Dal Corso, A.; de Gironcoli, S.; Fabris, S.; Fratesi, G.; Gebauer, R.; Gerstmann, U.; Gougoussis, C.; Kokalj, A.; Lazzeri, M.; Martin-Samos, L.; Marzari, N.; Mauri, F.; Mazzarello, R.; Paolini, S.; Pasquarello, A.; Paulatto, L.; Sbraccia, C.; Scandolo, S.; Sclauzero, G.; Seitsonen, A. P; Smogunov, A.; Umari, P.; Wentzcovitch, R. M Quantum Espresso: A Modular and Open-Source Software Project for Quantum Simulations of Materials. *J. Phys.: Condens. Matter* **2009**, *21*, 395502.
(23) Hybertsen, M. S.; Louie, S. G. Electron Correlation in Semiconductors and Insulators - Band-Gaps and Quasi-Particle Energies. *Phys. Rev. B: Condens. Matter Mater. Phys.* **1986**, *34*, 5390−5413.
(24) Deslippe, J.; Samsonidze, G.; Strubbe, D. A.; Jain, M.; Cohen, M. L.; Louie, S. G. BerkeleyGW: A Massively Parallel Computer Package for the Calculation of the Quasiparticle and Optical Properties of Materials and Nanostructures. *Comput. Phys. Commun.* **2012**, *183*, 1269−1289.
(25) Blum, V.; Gehrke, R.; Hanke, F.; Havu, P.; Havu, V.; Ren, X.; Reuter, K.; Scheffler, M. Ab Initio Molecular Simulations with Numeric Atom-centered Orbitals. *Comput. Phys. Commun.* **2009**, *180*, 2175−2196.

https://dx.doi.org/10.1021/jacs.9b13507
J. Am. Chem. Soc. 2020, 142, 3696−3700